Comments on "Narrow- and Broadband Satellite Measurements of Shortwave Radiation: Conversion Simulations with a General Circulation Model"

RACHEL T. PINKER AND ISTVAN LASZLO

Department of Meteorology, University of Maryland, College Park, Maryland

13 June 1987 and 28 January 1988

1. Introduction

Cess and Potter (1986) employed the Oregon State University/Lawrence Livermore National Laboratory (OSU/LLNL) general circulation model (GCM) as a tool for exploring various ways of converting narrowband measurements of solar radiation reflected from the earth–atmosphere system to broadband quantities.

Most satellites measure only the filtered earth atmosphere reflectance in narrow spectral intervals, and narrow solid angles. In the past, most satellite based radiation budget studies dealt with narrowband observations. Concern about a possible bias in the top of the atmosphere (TOA) radiation budgets, as derived from narrowband observations, lead to the design of special experiments whereby observations were taken over the whole solar spectrum [Nimbus-7; Earth Radiation Budget Experiment (ERBE)]. However, after the ERBE ends, operational satellites will continue to carry narrowband scanners. A basic understanding of the narrowband to broadband (n/b) relationship is crucial to all future attempts to monitor the earth's radiation budget (ERB), and to generate time series of long enough duration to address climate problems (e.g., interannual variability, and validation of climate model outputs). As pointed out by Cess and Potter (1986), in the past, emphasis has been given to the argument that ERB data are needed in order to validate numerical GCMs. The question whether the available ERB data are appropriate for such use is a timely one.

Few empirical and theoretical studies have been conducted in the past on the relationship between the spectral and total planetary reflectance [Smith et al. (1981); Minnis and Harrison (1984); Briegleb and Ramanathan (1982); Cess and Potter (1986); Pinker and Ewing (1986, 1987); Pinker (1987); Laszlo et al. (1987)]. Cess and Potter (1986; hereafter CP) were the first to address the problem of the narrowband/broadband relationship of shortwave radiation with a GCM model. They employed a modified version of the OSU/LLNL GCM to illustrate potential sampling errors associated with the use of narrowband detectors, and to test several different techniques for converting filtered albedos to unfiltered quantities. Their results indicate that it might be preferable to perform narrow- to broadband conversions in terms of planetary albedo (or an equivalent quantity) rather than in terms of reflected fluxes. They also demonstrated that the conversion could be improved if it was performed separately for clear and overcast regions. In their study the solar spectrum within the OSU/LLNL GCM was divided into three intervals ($\lambda < 0.5$ μm, 0.5 μm $\leq \lambda < 0.9$ μm, and $\lambda \geq 0.9$ μm). Because of this spectral resolution, a narrowband filter function was used consisting of a square-wave window extending from 0.5 to 0.9 μm. Furthermore, it was assumed that the reflectivities of the surfaces were independent of wavelength and direction; yet it is well known that land surface reflectivities have a significant spectral dependence. For vegetation this dependence is extremely strong in the narrow spectral interval that was considered by CP (e.g., Bowker et al. 1985). Both narrow- and broadband planetary albedos are likely to be affected by the properties of the surface reflectance even under cloudy conditions, provided the clouds are not too opaque. The purpose of this paper is to illustrate 1) the effect of the assumptions of wavelength and directional dependence on the conversion of narrowband to broadband albedos for cloudy scenes, and 2) the effect these assumptions might have on the conclusion of the study by CP.

2. Comment 1

Simulations of narrow- and broadband measurements of planetary albedos for cloudy scenes were performed with a modified version of a model developed by Pinker and Ewing (1985) for deriving surface global solar radiation from satellite observations. The modified version of the model was presented in Pinker and Laszlo (1987). The model was chosen since it provided an efficient way to calculate albedos for a relatively wide range of cloud optical thicknesses. In the model, the multiple scattering of molecules, aerosols and cloud droplets is computed by using the delta-Eddington ap-

Corresponding author address: Dr. Rachel T. Pinker, Department of Meteorology, University of Maryland, College Park, Maryland 20742.

TABLE 1. Land surface types of Briegleb et al. (1986) used in the simulations.

Type	Description	Identification in Fig. 2
1	Mixed farming, tall grassland	A
2A	Tall/medium grassland, evergreen shrubland	B
2B	Short grassland, meadow and shrubland	C
3	Evergreen forest (needleleaved)	D
4	Mixed decidious evergreen forest	E
5	Decidious forest	F
6	Tropical evergreen broadleaved forest	G
7	Medium/tall grassland, woodlands	H
8	Desert	I
9	Tundra	J

proximation of the radiative transfer (Wiscombe 1977). The absorption of ozone and water vapor is accounted for by using the parameterization of Lacis and Hansen (1974). The model has sufficient spectral resolution to incorporate what is presently known both on the spectral and the zenith angle dependence of reflectivities of natural surfaces. In our simulations the narrowband channels covered the wavelength interval of 0.5–0.7 μm, and the filter function, similarly to that of CP, was a square-wave window. For the reflectance of land surfaces, the models of Briegleb et al. (1986) were adopted. In these models the albedos of ten surface categories at four wavelength intervals of the solar spectrum are specified as a function of the solar zenith angle. The surface categories are summarized in Table 1. The surface wavelength and solar zenith angle dependence for types 8 and 9 (desert and tundra, respectively) are illustrated in Figure 1.

Simulations with wavelength independent and isotropic reflectors as lower boundaries of the atmosphere were also performed. The albedos of these surfaces were derived from the ratios of the spectrally integrated values of the reflected and incident fluxes at the surface. These fluxes were calculated using the spectral albedos of the models referenced above for the solar zenith angle of 60°, and the integration was carried out for the total shortwave interval. For both types of simulations the atmospheric conditions were the same (2 cm of precipitable water and 0.318 atm cm of ozone). For the extinction of aerosols the scattering parameters of a haze-*C* distribution (Leighton 1980) were adopted. The clouds were placed between atmospheric levels of 2 and 5.5 km. The optical properties of cloud droplets (extinction coefficient, single scattering albedo and asymmetry parameter) were derived by matching the reflectivities and absorptances of water clouds as derived from the parameterization of Stephens et al. (1984) with that derived from the delta-Eddington model.

In Fig. 2, the difference between the narrowband (0.5–0.7 μm) and the broadband (0.3–4.0 μm) albedo (hereafter (n-b)) is plotted as a function of cloud optical thickness, for different land surfaces and for the solar zenith angle of 60°. Results for (n-b) using wavelength and zenith-angle dependent surface reflectances are presented in Figure 2a. Results for (n-b) using isotropic and wavelength independent surface reflectances are

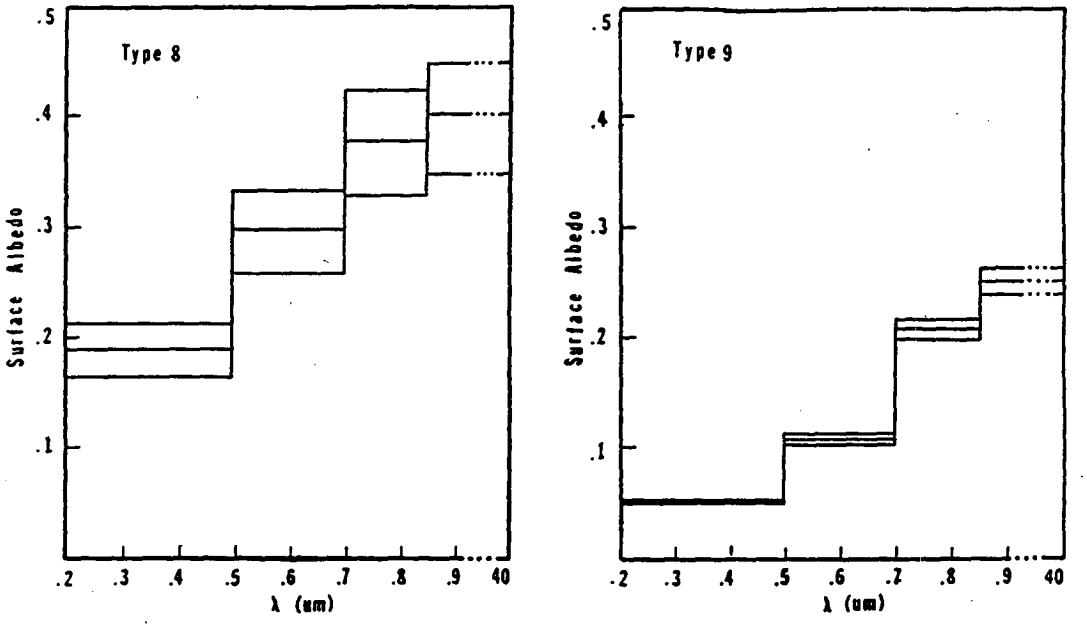

FIG. 1. Surface albedo variation as a function of wavelength and solar zenith angle for two surface types (8 and 9) as given in Table 1. The spread in the vertical represents the solar zenith angle dependence. Upper curves: 60°; middle curves: 45°; lower curves: 0°.

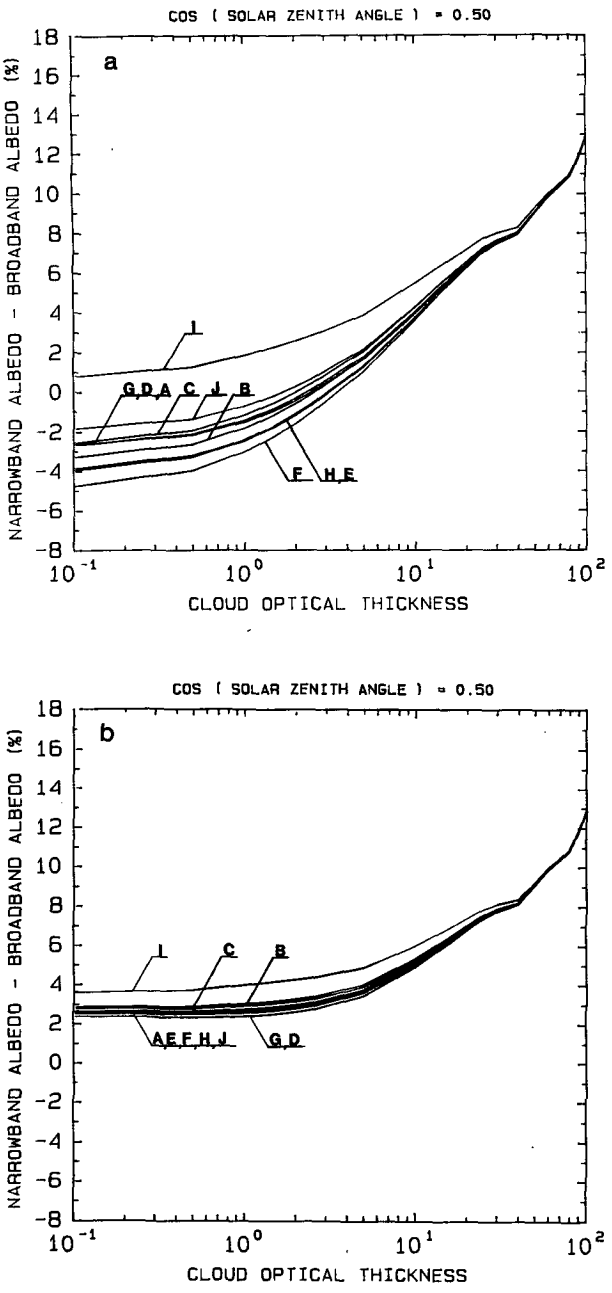

FIG. 2. The difference between narrowband (0.5–0.7 μm) and broadband (0.3–4.0 μm) planetary albedos as a function of cloud optical thicknesses for solar zenith angle of 60° and for ten surface types (identified by the letters A–J) as given in Table 1. Precipitable water amount = 2 cm; ozone amount = 0.318 atm cm. (a) Wavelength and solar zenith angle dependent surface reflectances; (b) isotropic and wavelength independent surface reflectances.

displayed in Fig. 2b. It is evident from the figure that even for cloudy scenes, the underlying surface can significantly affect both the narrow- and broadband albedos. This dependence on the surface types is evident up to a cloud optical thickness of about 25. Desert (I) can be "seen" through clouds of optical thickness up to about 70. Beyond this value, the wavelength and directional dependence of the surface reflectivities does not have an effect. Based on Fig. 2, the following observations can be made:

- The use of an isotropic surface with a constant surface reflectivity over the entire solar spectrum makes the albedo differences (n-b) less sensitive to the scene type. The spread of the curves is much smaller in Fig. 2b than in Fig. 2a, as could be expected. Without the atmosphere and with wavelength independent surface reflectivity, the broadband albedo would be equal to the narrowband albedo. The presence of the atmosphere causes some dispersion which is further increased by the spectral dependence of the surface reflectivity.
- The assumptions regarding the surface reflectivity affect the relationship between the narrow- and the broadband albedos. Simulations for surfaces with constant albedo (Figure 2b) show (n-b) to be positive for all optical thicknesses of clouds. Again, (n-b) would be zero for a surface with constant albedo if there was no atmosphere above it. Since clouds generally have higher albedos in the narrow spectral band of this study than in other parts of the spectrum, the (n-b) values are positive. On the other hand, since the narrowband albedos of vegetative land surfaces are about 30%–60% less than the broadband ones (Briegleb et al. 1986), the (n-b) values are negative for thin clouds if the surface model includes wavelength and directional dependence. With the increase of the cloud optical thickness, the influence of the surface decreases, and for a thick cloud, (n-b) is the same regardless of the surface model. This would imply that if one applied linear regressions for both types of simulations, the slope of the regression line derived from the simulations with the realistic surface models would be larger than the one obtained from the simulations with constant surface albedos.

As pointed out by others (e.g., Shine et al. 1984; Hartmann et al. 1986), the narrowband visible (0.5–0.7 μm) albedo strongly overestimates the broadband albedo in the presence of clouds. The same conclusion can be drawn from the results presented in Fig. 2b, where the surface albedos were assumed to be solar zenith angle and wavelength independent. However, from the results presented in Fig. 2a, it is evident that the broadband albedo can be underestimated by the narrowband albedo if the cloud is not too thick. Since the constant albedos were derived from integrated spectral reflectances at solar zenith angle of 60°, the differences between Figs. 2a and 2b are indicative of the wavelength dependence of the surface reflectivities.

3. Comment 2

This comment concerns the conclusion of CP regarding the preference of conversion in terms of albedos

to those in terms of fluxes. It is based on simulations that were performed with the spectrally and vertically detailed radiative transfer code ATRAD developed by Wiscombe (e.g., Wiscombe et al. 1984). The code employs the adding-doubling technique for calculating multiple scattering, and accounts for the absorption of all known atmospheric gases. The total shortwave spectrum is divided into 185 intervals. A variety of atmospheres and surfaces including the standard atmospheres of McClatchey (Kneizys et al. 1980), the standard aerosol models (WCP-55 1983), the cloud models of Stephens (1979) and the surface models of Briegleb et al. (1986) were considered. A detailed description of the simulations is presented in Laszlo et al. (1987).

The scatter diagram of the narrow- versus broadband albedos is shown in Fig. 3. The narrowband filter function used was the same as used by CP (square-window between 0.5–0.9 μm). The scene types are identified as follows: 1, ocean; 2, vegetation; 3, desert; 4, clouds with various liquid water content; 5, snow. For a given surface type, the atmosphere (water vapor, ozone, aerosol, temperature, pressure, etc.) and the solar zenith angle were varied. In Fig. 4, the filtered fluxes were plotted versus the broadband fluxes. The filtered fluxes were derived, like in CP, by multiplying the narrowband albedo by the total solar irradiance at the top of the atmosphere. Note that in the albedo plot (Fig. 3) the points for scenes of relatively low reflectivities (ocean, vegetative land, desert and not very deep clouds) are along a straight line. The points for deep clouds and snow, however, show wide scatter, indicating that a linear fit of these albedos would give less accurate estimates of the broadband albedo than it does for the other surfaces. In contrast, the flux plot (Fig. 4) shows an improvement indicating that for these scenes, a linear regression on the filtered fluxes is more adequate than that on the albedos. It can also be seen that for dark scenes (ocean and vegetative land), the scatter around a regression line is smaller for albedos than that for fluxes. This suggests a preference for albedo regression to a flux regression for these surfaces. A similar conclusion was obtained by Wiscombe (personal communication, 1983), who used ATRAD results for aerosol-free atmospheres with selected surfaces, and considered a spectral band of 0.5–0.7 μm only.

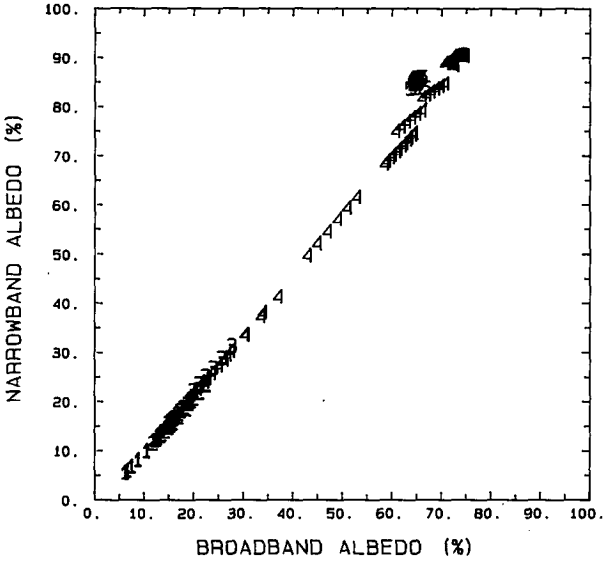

FIG. 3. Scatter diagram of narrowband/broadband planetary albedo for the following five scenes: 1, ocean; 2, vegetative lands; 3, desert; 4, clouds; 5, snow. For each scene, characteristic atmospheric constituents were used. Variation in the solar zenith angle (between 0°–60°) was also included.

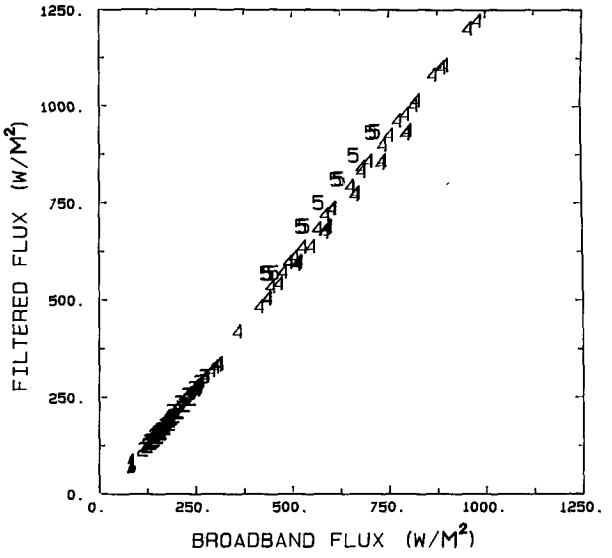

FIG. 4. As in Fig. 3, except for filtered reflected/broadband flux.

For quantitative analysis, linear regression equations were derived for each of the five scene types (ocean, vegetative land, desert, clouds, and snow) separately. The linear regressions were performed both on the albedos (hereafter, regression A) and on the filtered fluxes (regression B). The correlation coefficients are presented in Table 2. Following CP, a correlation between the so-called unfiltered fluxes and the broadband fluxes

TABLE 2. Correlation coefficients from regressions A, B and method C.

Surface type	Correlation coefficients: Regressions A	Regressions B	Method C
Ocean	0.9994	0.9076	0.9218
Vegetated land	0.9951	0.9942	0.9984
Desert	0.9998	0.9999	0.9998
Clouds	0.9981	0.9985	0.9985
Snow	0.2138	0.9984	0.9982

was also established (method C). The albedo conversions derived from Fig. 3 were used to predict the broadband albedos. Multiplying these predicted broadband albedos by the total solar irradiance yields the unfiltered fluxes. The scatter diagram of these fluxes is shown in Fig. 5. The correlation coefficients between the unfiltered and the broadband fluxes are also included in Table 2. Correlations between unfiltered and broadband fluxes could also be established by using the linear flux regressions of Figure 4. The coefficients of such correlations would be identical to those produced by regression B. Comparing the correlation coefficients in Table 2, the following can be observed:

- In terms of unfiltered fluxes, method C is better than or comparable to regression B for all surface types considered in the simulations. The differences in the correlation coefficients of the two methods are small for desert and clouds.
- The correlation between narrow- and broadband albedo (regression A) is higher for ocean than that between the narrow- and broadband fluxes (regression B). The situation is the opposite for snow, and the difference between the correlation coefficients of the two types of regressions is the largest. This is primarily due to the fact that the variation in the albedo of snow is small (Fig. 3), while that in the reflected flux is much larger (Fig. 4). By contrast, the variation in the ocean albedo is larger than that in the reflected flux. The latter discussion does not contradict the conclusion of the study by CP, since the CP study is based on the comparison of regression B with method C.

4. Summary

It has been demonstrated that applying a high spectral resolution radiative transfer model and spectral-directional dependent surface reflectances leads to the same conclusion as reached by CP in their simulations of n/b transformations. Our results also support the preference of performing n/b conversion in terms of planetary albedos (method C), rather than in terms of reflected fluxes (regression B). However, it has been shown that the differences between these two methods are significant only for relatively dark surfaces (ocean and vegetation). The results also indicate that relatively simple radiative transfer models (like the one used by CP) coupled with the assumption of a constant surface albedo can contribute to a better understanding of the conversion of narrowband satellite measurements to broadband quantities. It has been demonstrated, however, that for deriving regression equations from simulations, the inclusion of "realistic" surface models is crucial even in the presence of clouds.

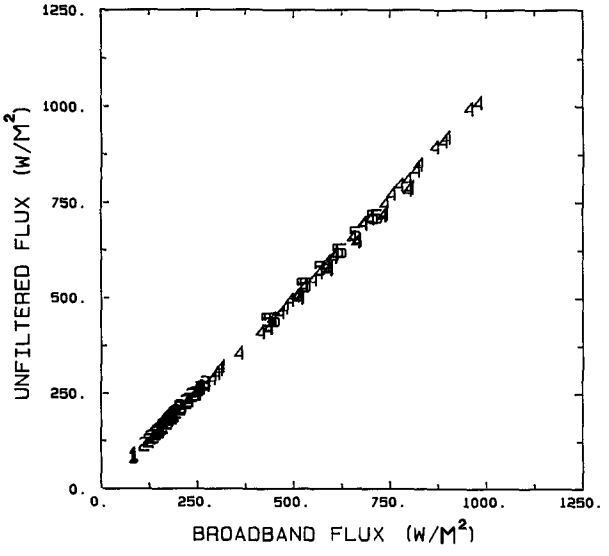

FIG. 5. As in Fig. 3, except for unfiltered reflected/broadband flux.

Acknowledgments. This work was supported by Grant NAG-5-914 from the National Aeronautics and Space Administration, Earth Science and Applications Division, Climate Research Program, to the University of Maryland.

REFERENCES

Bowker, D. E., R. E. Davis, D. L. Myrick, K. Stacy and W. T. Jones, 1985: Spectral reflectances of natural targets for use in remote sensing studies. NASA Ref. Pub. 1139, 184 pp.

Briegleb, B. P., and V. Ramanathan, 1982: Spectral and diurnal variations in clear-sky planetary albedo. *J. Appl. Meteor.*, **21**, 1160–1171.

——, P. Minnis, V. Ramanathan and E. Harrison, 1986: Comparison of regional clear-sky albedos inferred from satellite observations and model calculations. *J. Climate Appl. Meteor.*, **25**, 214–226.

Cess, R. D., and G. L. Potter, 1986: Narrow- and broadband satellite measurements of shortwave radiation: Conversion simulations with a General Circulation Model. *J. Climate Appl. Meteor.*, **25**, 1977–1984.

Hartmann, D. L., V. Ramanathan, A. Berrior and G. E. Hunt, 1986: Earth radiation budget data climate research. *Rev. Geophys.*, **24**, 439–468.

Kneizys, F., E. Shettle, W. Gallery, J. Chetwynd, L. Abreu, J. Selby, R. Fenn and R. McClatchey, 1980: Atmospheric transmittance/radiance: Computer code LOWTRAN5. Rep. AFGL-TR-80-67, Air Force Geophysics Laboratory, Hanscom AFB, MA, 127 pp.

Lacis, A. A., and J. E. Hansen, 1974: A parameterization for the absorption of solar radiation in the earth's atmosphere. *J. Atmos. Sci.*, **31**, 118–133.

Laszlo, I., H. Jacobowitz and A. Gruber, 1987: The relative merits of narrowband channels for estimating broadband albedos. *J. Atmos. Oceanic Technol.* (in press).

Leighton, H. G., 1980: Application of the delta-Eddington method to the absorption of solar radiation in the atmosphere. *Atmos. Ocean*, **18**, 43–52.

Minnis, P., and E. F. Harrison, 1984: Diurnal variability of regional cloud and clear-sky radiative parameters derived from GOES data. Part III: November 1978 radiative parameters. *J. Climate Appl. Meteor.*, **23**, 1032–1051.

Pinker, R. T., 1987: Simulations of the METEOSAT visible sensor responses to changing boundary conditions. *Adv. Space Res.*, **7**, 211–216.

——, and J. A. Ewing, 1985: Modeling surface solar radiation: Model formulation and validation. *J. Climate Appl. Meteor.*, **24**, 389–401.

——, and ——, 1986: Effect of surface properties on the narrow- to broadband relationship in satellite observations. *Remote Sens. Environ.*, **20,** 267–282.

——, and ——, 1987: Simulation of the GOES VISSR sensor to changing surface and atmospheric conditions. *J. Geophys. Res.*, **92,** D4, 4001–4009.

——, and I. Laszlo, 1987: An improved model for surface solar radiation from satellite observations. IAMAP/IUGG Meeting, Vancouver, August 9–22, 1987.

Shine, K. P., A. Henderson-Sellers and A. Slingo, 1984: The influence of the spectral response of satellite sensors on estimates of broadband albedo. *Quart. J. Roy. Meteor. Soc.*, **110,** 1170–1179.

Smith, W. L., L. D. Herman, T. Schreiner, H. B. Howell and P. Menzel, 1981: Radiation budget characteristics of the onset of the Summer Monsoon. *International Conference on Early Results of FGGE and Large-Scale Aspects of its Monsoon Experiments*, IAMAP/WMO/AMS, Tallahassee, FL.

Stephens, G. L., 1979: Optical properties of eight water cloud types. Commonwealth Scientific and Industrial Research Organization, Division of Atmospheric Physics, Technical paper No. 36, Australia, 18–26.

——, S. Ackerman and E. Smith, 1984: A shortwave parameterization revised to improve cloud absorption. *J. Atmos. Sci.*, **41,** 687–690.

WCP-55, 1983: *World Climate Research report of the experts meeting on aerosols and their climatic effects.* Williamsburg, Virginia, 28–30 March 1983, A. Deepak and H. E. Gerber, Eds., 107 pp.

Wiscombe, W. J., 1977: The delta-Eddington approximation for a vertically inhomogeneous atmosphere. NCAR Tech. Note 121, 1–66.

——, R. M. Welch and W. D. Hall, 1984: The effects of very large drops on cloud absorption. Part I: Parcel models. *J. Atmos. Sci.*, **41,** 1336–1355.